RSC Advances

PAPER

View Article Online
View Journal | View Issue

Cite this: *RSC Adv.*, 2025, **15**, 17811

Nanoporous $[Ho_2(CO_2)_7(H_2O)_2]$-organic frameworks for excellent catalytic performance on the cycloaddition of CO_2 into epoxides and the deacetalization-Knoevenagel condensation†

Tao Zhang,[a] Shujun Liang,[a] Shuai Jia,[a] Haibo Cui,[a] Xinyi Wang[a] and Xiutang Zhang *[b]

Designing nanoporous lanthanide-based metal–organic frameworks (MOFs) as robust heterogeneous catalysts has received a lot of interest in recent years. Herein, we successfully constructed a novel isomorphic nanoporous MOF $\{[Ho_2(TDP)(H_2O)_2]\cdot 5H_2O\cdot 4DMF\}_n$ (named as **NUC-55**, NUC = North University of China) by combining $[Ho_2(CO_2)_7(H_2O)_2]$ (abbreviated as $\{Ho_2\}$) clusters with 2,4,6-tri(2,4-dicarboxyphenyl)pyridine (H_6TDP) as structure-oriented multifunctional ligands under acidic solvothermal conditions. **NUC-55** is a holmium(III)-based 3D MOF with a hierarchical porous architecture containing tetragonal microchannels (0.56 nm in diameter) and octagonal nanochannels (1.79 nm in diameter), In **NUC-55**, plenty of Lewis acidic and basic sites, including open Ho^{3+} sites and $N_{pyridine}$ atoms, coexist. Moreover, it is worth mentioning that the void volume (~65%) is significantly higher in **NUC-55** than in most documented 3D lanthanide-based MOFs (Ln-MOFs). Catalytic experiments show that activated **NUC-55** exhibits high catalytic activity in the CO_2–styrene oxide cycloaddition reactions under mild conditions, with a high turnover number of 2475 and a high turnover frequency of 619 h^{-1}. In addition, activated **NUC-55** can remarkably accelerate the deacetalization-Knoevenagel condensation reactions of benzaldehyde dimethyl acetal and malononitrile. Taken together, this work can not only establish an effective self-assembly strategy for fabricating highly porous Ln-MOFs, but also provide new insights into their catalytic mechanism.

Received 1st April 2025
Accepted 23rd May 2025

DOI: 10.1039/d5ra02269j

rsc.li/rsc-advances

1 Introduction

Metal–organic frameworks (MOFs), which are formed by combining inorganic secondary building units (SBUs) and organic ligands, have a wide range of applications in various fields, such as gas separation-storage,[1,2] heterogeneous catalysis,[3,4] fluorescent sensors and probes,[5,6] and sustained drug-releasing systems.[7] Nowadays, with the development of MOF chemistry, porous materials with pores of different sizes and shapes have been successfully fabricated by changing their structural units, leading to improved physicochemical properties and wider applications.[8–10] Although the specific structure of ligands connecting inorganic components into modularly assembled complex superstructure is most exciting, it remains challenging to establish a predictable synthetic route to assemble with a specific chemical composition and function of the topological structure of target materials. Therefore, a systematic exploration of predictable synthetic pathways and characterization of MOFs is still needed[11,12].

In recent years, excess carbon dioxide (CO_2) in the atmosphere has caused great damage to the ecosystem, such as rainstorms, floods, mudslides, and landslides.[13–16] Therefore, researchers are developing various technologies to capture and convert CO_2 into energy products. Among them, CO_2-epoxide cycloaddition (CEC) has attracted extensive attention, because the generated cyclic carbonate can be widely used in green solvents, lithium batteries, polymers, chemical intermediates, and so on.[17–20] However, some limitations, such as slow reaction rates and lack of efficient catalysts, restrict the application of CEC in CO_2 capture and fixation. Thus, it is very important to develop recyclable high-performance heterogeneous catalysts under mild conditions.[21,22] Recently, MOFs have been considered one of the most promising heterogeneous catalysts for the

[a]*Department of Materials Engineering, Taiyuan Institute of Technology, Taiyuan 030008, P. R. China*

[b]*School of Chemistry and Chemical Engineering, North University of China, Taiyuan 030051, P. R. China. E-mail: xiutangzhang@163.com*

† Electronic supplementary information (ESI) available: Experimental section, X-ray data for **NUC-55**. Crystallographic data and refining parameters of **NUC-55**. Selected bond lengths and angles. The TGA curves of as-synthesized and activated **NUC-55** sample. PXRD patterns of **NUC-55** after water treatment. N_2 absorption/desorption isotherms of **NUC-55** at 77 K. CCDC 2125269. For ESI and crystallographic data in CIF or other electronic format see DOI: https://doi.org/10.1039/d5ra02269j

CEC owing to the presence of easily accessible Lewis acidic and/or basic sites and highly tunable porosity. Many transition metal-based MOFs have been developed, such as ZIF-67,[23] gea-MOF-1,[24] BIT-103,[25] USTC-253,[26] MIL-101,[27] MOF-505,[28] and UIO-66.[29] However, due to the lack of effective synthetic strategies, there are few reports on lanthanide-based MOFs (Ln-MOFs). In fact, Ln-MOFs are expected to exhibit more excellent catalytic activity because of the strong Lewis acidity of Ln^{3+} ions, as evidenced by Friedel–Crafts,[30] Diels–Alder,[31] aldol–allylation,[32] and Michael addition reactions.[33] Thus, in order to construct highly catalytic Ln-MOFs, there is an urgent need to develop effective synthetic strategies for building large-pore and high-surface-area structures to facilitate the interactions between Ln^{3+} ions and organic ligands.[34–38]

In this study, 2,4,6-tri(2,4-dicarboxyphenyl)pyridine (H_6TDP) was used as a difunctional N-containing heterocyclic ligand to construct Ln-MOFs with the ability to catalyze the CEC under mild conditions (101.32 kPa, low temperatures). Here, we successfully fabricated a dual-channel Ho-based MOFs ($\{[Ho_2(TDP)(H_2O)_2]\cdot 5H_2O\cdot 4DMF\}_n$, **NUC-55**), which processed excellent physico-chemical properties, such as high porosity, large specific surface areas, solvent-free dual channels, thermal stability, and solvent tolerance. Because of the coexistence of Lewis acidic and basic sites, such as Ho^{3+} ions, N=O and C=O groups, and $N_{pyridine}$ atoms, **NUC-55** exhibited very high catalytic activity in the cycloaddition of CO_2 with styrene oxide under solvent-free and mild conditions. Moreover, **NUC-55** could remarkably accelerate the deacetalization-Knoevenagel condensation of various substrates.

2 Results and discussion

2.1 Crystal structure

Based on single crystal X-ray diffraction analysis, **NUC-55** crystallizes in the tetragonal space group $P4_322$ and processes a dinuclear hierarchical porous framework formed by combining $[Ho_2(CO_2)_7(H_2O)_2]$ SBUs and 4-connected TDP^{6-} moieties. PLATON calculation shows that there are two kinds of edge-sharing channels, including tetragonal micropores (*ca.* 0.56 nm) and octagonal nanopores (*ca.* 1.79 nm), leading to a total potential solvent-accessible void volume of *ca.* 4489.1 $Å^3$ and a porosity of 64.9%, which are larger than those of other 3D Ln-MOFs, such as $\{Ln(BTB)\}_n$ (49.6%),[39] $\{[Pr_3(ATPT)_2(HATPT)_4(NO_3)(H_2O)_8]_n\}$ (47.9%),[40] $Er_2(TBDC)_3(phen)_2$ (38.9%),[41] $\{Ln(TPO)\}_n$ (48.4–49.0%),[42] $\{Ln_3(PTTBA)_2\}_n$ (51.2%),[43] and **NUC-38** (56.3–56.7%).[44] It's worth noting that **NUC-55** can act as a Lewis acid catalyst since the unoccupied coordination sites associated with each Ho^{3+} ion in octagonal-nanoporous channels can be converted to defective hexa-coordination configuration after releasing water molecules. Furthermore, Lewis basic sites (*i.e.*, uncoordinated $N_{pyridine}$ atoms) are found on the internal surface of microporous channels. Thus, **NUC-55** is an ideal candidate for gas separation/reservoir, catalysis, and fluorescence recognition.

In **NUC-55**, two Ho^{3+} ions are spanned together by three μ_2–η^1:η^1 carboxyl groups from three separate TDP^{6-} moieties to form a $[Ho_2(CO_2)_7(H_2O)_2]$ cluster (abbreviated as $\{Ho_2\}$, Fig. 1a),

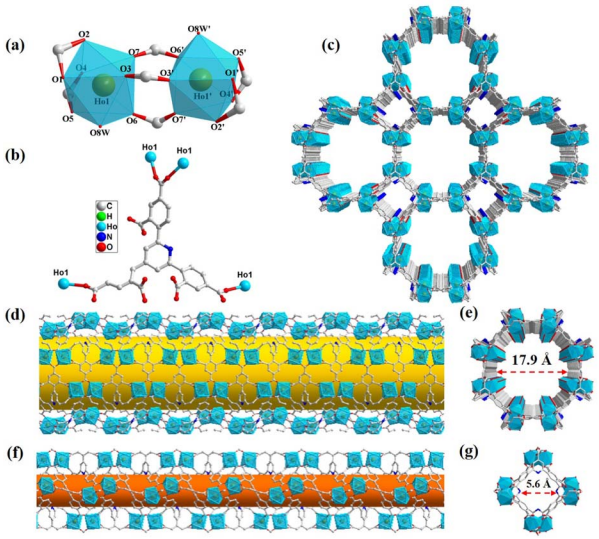

Fig. 1 (a) $[Ho_2(CO_2)_7(H_2O)_2]$ SBUs and its simplified design. (b) The asymmetrical unit of **NUC-55**. (c) The neutral dual-channel framework of **NUC-55**. (d) Schematic diagram of the three-dimensional structure of channel I. (e) Side view of channel I. (f) Schematic diagram of the three-dimensional structure of channel II. (g) Side view of channel II.

which is subsequently caught by five TDP^{6-} moieties (Fig. 1b) to propagate into a rare 3D Ho–organic framework (Fig. 1c), with a potential solvent-accessible volume of 4489.1 $Å^3$ calculated by PLATON program.[45,46] In **NUC-55**, each of eight rows of $\{Ho_2\}$ clusters with the aid of ambient carbon framework was built into a hydrophilic 1D octagon channel **I** (Fig. 1d), with a diameter of 1.79 nm (Fig. 1e), indicating the presence of nearly mesoporous channels in **NUC-55**. For channel II (Fig. 1f and g), four $\{Ho_2\}$ clusters are connected through two completely deprotonated ligands to generate a 1D square-shaped channel that is hydrophobic and has an inner diameter of 0.56 nm. Meantime, a 3D ultramicroporous architecture is formed by assembling two types of channels along the *c* axis in an edge-sharing way (Fig. 1c). In addition, the hexapodal TDP^{6-} ligand exhibits a self-adaptive behavior in the non-structural deformation due to three dihedral angles (46.4°, 40.0°, and 47.5°) among three branched benzene plane and the central pyridine.

Based on topological analysis,[47,48] the neutral host framework of **NUC-55** can be simplified into a 3D nut-type (4,5)-c network with the Schläfli symbol of $(3^2\cdot 4^2\cdot 5^2)(3^4\cdot 4^3\cdot 5^4\cdot 6^9\cdot 7)$ by taking TDP^{6-} moieties and $\{Ho_2\}$ clusters as a linear 5-connected triangle and a 4-connected octahedron, respectively (Fig. S3†).

2.2 Gas adsorption performance

The PXRD patterns of **NUC-55** show that the phase purity is very high (Fig. S4†). To test the gas adsorption performance, **NUC-55** was activated by exchanging it with methanol three times, with methanol renewed every 24 h, and dried in a vacuum oven at 80 °C for 24 h. The characteristic diffraction peaks in the PXRD pattern of activated **NUC-55** were highly consistent with those of the as-synthesized samples (Fig. S5†), indicating that **NUC-55**

has excellent stability after desolvation. The N_2 adsorption isotherm of **NUC-55** at 77 K (Fig. S6†) shows that the permanent porosity increases sharply at low pressures of 0–0.2 bar (Fig. S6†), indicating that it belongs to a typical type I adsorption–desorption isotherm. The overall N_2 uptake of **NUC-55** at 1 atm was 305 $cm^3\ g^{-1}$. The Brunauer–Emmett–Teller (BET) surface area and Langmuir surface area are 1214 and 1547 $m^2\ g^{-1}$, respectively. We used non-local density functional theory to fit the N_2 adsorption isotherm at 77 K, and the results showed that the pore sizes of **NUC-55** were concentrated at 0.58 nm and 1.72 nm (Fig. S7†), which were consistent with those obtained from the crystal structure.

Furthermore, the CO_2 adsorption curve of **NUC-55** was a typical type I adsorption isotherm at 273 K and 298 K, and the maximum volumetric uptakes of CO_2 were 120.3 and 59.3 $cm^3\ g^{-1}$, respectively (Fig. S8†). The accurate prediction of CO_2 adsorption at the saturation point was obtained by fitting isotherms measured at 273 and 298 K using the same method. At low coverage, the estimated isosteric heat of adsorption (Q_{st}) for **NUC-55** was 23.5 kJ mol^{-1} (Fig. S9†), indicating that the adsorption of CO_2 by **NUC-55** is mainly physical adsorption. Because of the low heat of adsorption, it was easy for **NUC-55** to be regenerated through desorption at low temperatures.

2.3 Catalytic cycloaddition of CO_2 to styrene oxide under mild conditions

Activated **NUC-55** had many merits as follows. (i) After losing coordinated solvent molecules, Ho^{3+} ions can be used as Lewis acidic active sites to activate small molecules with unbalanced charge distributions. (ii) Uncoordinated pyridine groups can be used as complementary catalytic sites for CO_2 cycloaddition. (iii) Nanoscale pores can facilitate the mass transfer of substrates. The catalytic effect of **NUC-55** on the CEC was studied using styrene oxide as the standard substrate. The yield of the products was quantitatively analyzed using GC-MS. The structure of the products was determined using NMR (Fig. S10†). Particularly, the synergistic effect of *n*-Bu_4NBr as a cocatalyst for **NUC-55** was also tested. As shown in Table 1, the conversion of styrene oxide was very low in the presence of only a single catalyst in 48 h (entries 1 and 2). In contrast, in the presence of both 0.10 mol% **NUC-55** and 5 mol% *n*-Bu_4NBr, the yield increased to 27% at room temperature only in 8 h (entry 3). With the prolongation of reaction time from 16 to 48 h, the yield increased significantly from 45% to 96% (entries 4–8), indicating that *n*-Bu_4NBr could synergistically improve the conversion efficiency of CO_2 since free Br^- ions could polarize the β-carbon on ethylene oxide through nucleophilic attack to initiate the ring–opening reaction of epoxides. Next, we observed the effects of reaction time, reaction temperature, and catalyst dosage on the catalytic performance. When the reaction time was extended to 48 h (entries 3–8), the conversion rate reached 96%. Interestingly, as the reaction temperature increased from 35 to 80 °C (entries 9–14), the reaction could be almost completed at a very short reaction time (4 h). At 0.04–0.10 mol% of **NUC-55**, the dosage had little effect on the catalytic performance (entries 14–17). However, at doses of **NUC-55** below 0.02 mol%, the yield decreased significantly (entry 18–19). Therefore, the optimal reaction conditions for the cycloaddition of CO_2 with epoxides were selected as follows: 80 °C, $P_{CO_2} = 1$ atm, 0.04 mol% **NUC-55**, and 5 mol% *n*-Bu_4NBr. It is noteworthy that the catalytic efficiency of **NUC-55** for styrene oxide is much higher than those of most reported MOF catalysts, such as Zn-2PDC,[49] Rh-PMOF-1,[50] and JLU-MOF58 (Zr) (Table S4†).[51]

2.4 Cycloaddition of CO_2 with various epoxides

To test the catalytic ability of **NUC-55**, 10 typical epoxides with different steric hindrance groups and electron-withdrawing (or donating) groups were selected for the cycloaddition reaction with CO_2 under the optimal conditions (Table 2). **NUC-55** had high catalytic activity for epoxides with small steric hindrance. The structures of all cycloaddition products were characterized using ^1H NMR and ^{13}C NMR (Fig. S11–S19†). However, styrene oxide (entry 9) and 3-phenoxy-1,2-epoxypropane (entry 10) were not easily dispersed in the nanochannels of **NUC-55** due to their large steric hindrance, so they could not be effectively activated at the exposed catalytic sites, leading to a slight decrease in the yield. In addition, the molecular sizes of epoxides varied with different substituted groups (Table S3†). In comparison with several MOF-based catalysts reported in the literature (Table S5†), we found that **NUC-55** exhibited higher catalytic activity against an epoxide with a bulky substituted group, indicating that **NUC-55** might had a wider application.

2.5 Recyclability and stability of NUC-55 in CO_2-epoxide cycloaddition

The recyclability and stability of **NUC-55** in cycloaddition reactions were also investigated under optimal conditions. After each reaction, organic matter adsorbed to **NUC-55** was removed by immersing **NUC-55** in ethyl acetate, followed by vacuum drying. During five catalytic cycles of **NUC-55**, the yields ranged between 96% and 99% (Fig. S20†), indicating that **NUC-55** had excellent catalytic performance, high recyclability and stability. Furthermore, after 5 catalytic cycles, recycled **NUC-55** exhibited similar characteristic PXRD peaks to those of original **NUC-55**, indicating that the structure of **NUC-55** remained unchanged after 5 catalytic cycles (Fig. S21†). This can be observed from the SEM images before and after CO_2 cyclization reaction catalyzed by **NUC-55** (Fig. S22†). The N_2 adsorption capacity of recycled **NUC-55** was 286 $cm^3\ g^{-1}$(Fig. 2), which was slightly less than 302 $cm^3\ g^{-1}$ of original **NUC-55**, possibly due to the blockage of pores and channels by residual styrene carbonate. In addition, the result obtained from ICP-MS showed that only a small amount of Ho^{3+} ions (0.016%) were leached from **NUC-55**, further confirming the excellent stability of **NUC-55**. Finally, the heterogeneity of **NUC-55** was verified by the thermal filtration experiment (Fig. S23†). Once **NUC-55** was removed from the reaction system after 2 h of reaction, the yield did not increase, indicating that the catalytic reaction was terminated, which confirms that **NUC-55** possessed pure heterogeneous properties.

Table 1 CO_2–styrene oxide cycloaddition under different conditions[a]

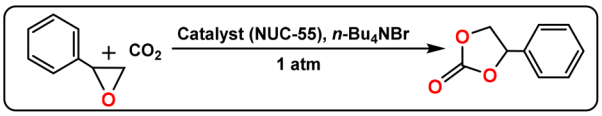

Entry	NUC-55 (mol%)	n-Bu_4NBr (mol%)	Temp. (°C)	Time (h)	Yield[b] (%)	TON[c]	TOF[d]
1	0	5	RT	48	13	—	—
2	0.10	0	RT	48	9	90	2
3	0.10	5	RT	8	27	271	34
4	0.10	5	RT	16	45	450	28
5	0.10	5	RT	24	64	640	26
6	0.10	5	RT	32	77	770	24
7	0.10	5	RT	40	90	900	221
8	0.10	5	RT	48	96	960	20
9	0.10	5	35	40	98	980	25
10	0.10	5	40	32	99	990	31
11	0.10	5	50	24	99	990	41
12	0.10	5	60	12	99	990	83
13	0.10	5	70	8	99	990	124
14	0.10	5	80	4	100	1000	249
15	0.08	5	80	4	99	1238	311
16	0.06	5	80	4	99	1650	413
17	0.04	5	80	4	99	2475	619
18	0.02	5	80	4	92	4600	1150
19	0	5	80	4	53	—	—

[a] Reaction conditions: solvent free, styrene oxide (20 mmol), and CO_2 (1 atm). [b] Product yield was determined using GC-MS with n-dodecane as an internal standard. [c] TON (turnover number): mole of product/mole of catalyst. [d] TOF (turnover frequency): TON/time. RT: room temperature.

2.6 Possible mechanism of the catalytic activity of NUC-55 in the cycloaddition of CO_2 into epoxides

By combining previous studies[41,52] and the structural features of **NUC-55**, we proposed a possible catalytic mechanism for **NUC-55** to promote the cycloaddition of CO_2 into epoxides (Fig. 3). The catalytic process is composed of four steps, including polarization, loop opening, insertion, and loop closing. (i) Ethylene oxide is activated by Ho^{3+} ions after adsorption to its oxygen atoms. (ii) The loop was opened when nucleophilic Br^- anions attacked carbon atoms in epoxides with small steric hindrance and generated alkylcarbonate anions.[53–57] (iii) CO_2 molecules adsorbed in the channels of **NUC-55** were polarized and inserted into alkylcarbonate anions because of their electronic equilibrium and stability at the ground state.[58–62] (iv) Finally, the loop was closed, and one cycle of the reaction ended and the next one began.

2.7 Catalytic performance of NUC-55 for deacetalization-Knoevenagel condensation

The catalytic performance of **NUC-55** for deacetalization-Knoevenagel condensation was tested given the coexistence of Lewis acidic and basic sites, including Ho^{3+} ions, carbonyl oxygen atoms, and pyridinyl groups.[25,63–66] Using benzaldehyde dimethyl acetal (BDA) and malononitrile as model reactants and DMSO as a solvent, the effects of reaction temperature, reaction time and catalyst dosage on the catalytic performance were investigated. When the reaction was carried out at 40 °C for 12 h, the yields increased gradually from 3% to 76% as the doses of **NUC-55** increased from 0 to 0.30 mol% (entries 2–6, Table 3), indicating that **NUC-55** exerted catalytic effects on the deacetalization-Knoevenagel condensation reaction. At 55 °C, the yield reached 96.22% in 12 h, however, the yield could reach 99.33% in 6 h at 70 °C. These results indicated that **NUC-55** had high catalytic effects on the tandem deacetalization-Knoevenagel condensation under the optimal condition (0.30 mol% **NUC-55**, temperature: 70 °C, and reaction time: 6 h). Moreover, compared with other MOFs reported in the literature (Table S7†) **NUC-55** had higher catalytic efficiency for the Knoevenagel condensation of BDA.

2.8 Substituted groups and size selectivity in the deacetalization-Knoevenagel condensation reaction

The deacetalization-Knoevenagel condensation reactions were carried out using various BDA derivatives containing different electron acceptors (–NO_2, –F, and –Br) and electron donors (–CH_3, –OCH_3, and –OPh) under the optimal condition. As shown in Table 4, **NUC-55** could catalyze the condensation reaction of all BDA derivatives tested. However, it is noted that different substituted groups could affect the reaction to a certain extent, and the yields were slightly higher for BDA derivatives with electron acceptors than those with electron donors. In addition, adverse effects on the electron-donating groups could be verified by several substituted groups, such as –OCH_3 and –OPh (entries 7–10). Moreover, molecular size is also an important

Table 2 Cycloaddition of CO_2 with various epoxides with NUC-55[a]

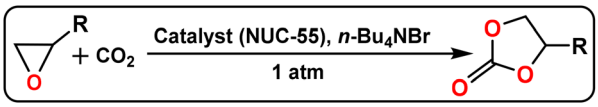

Entry	Epoxides	Selectivity (%)	Yield[b] (%)	TON[c]
1		99	99	2475
2		99	99	2475
3		99	99	2475
4		99	99	2475
5		99	99	2475
6	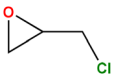	99	99	2475
7	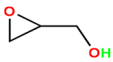	98	99	2475
8		99	99	2475
9	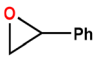	99	98	2450
10	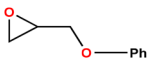	97	95	2375

[a] Reaction conditions: substrates (20 mmol), n-Bu_4NBr (5 mol%), NUC-55 (0.04 mol%, based on the {Ho_2} cluster), CO_2 (1 atm), 80 °C, and 4 h. [b] n-Dodecane was used as the internal standard and determined by GC-MS. [c] TON (turnover number) = mole of product/mole of catalyst.

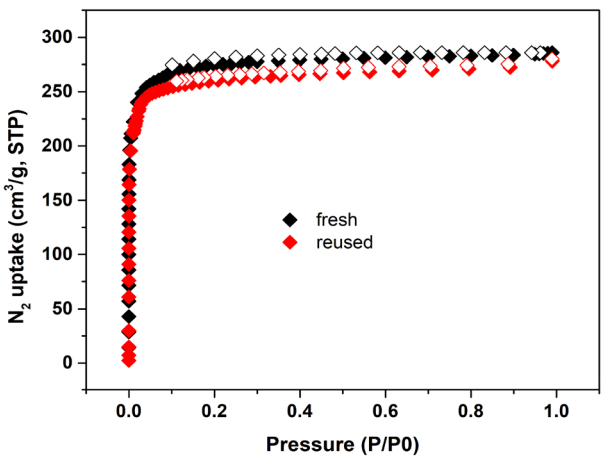

Fig. 2 N_2 adsorption isotherms of NUC-55 before and after five catalytic cycles.

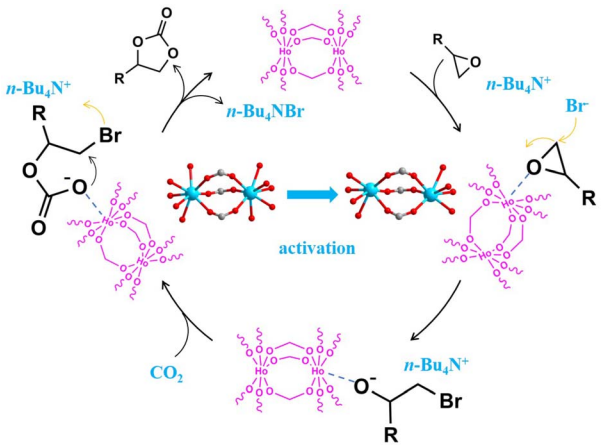

Fig. 3 Proposed mechanism of NUC-55 to catalyze the cycloaddition of CO_2 into epoxides.

Table 3 Catalytic Effects of NUC-55 on the deacetalization-Knoevenagel condensation reaction between benzaldehyde dimethyl acetal and malononitrile[a]

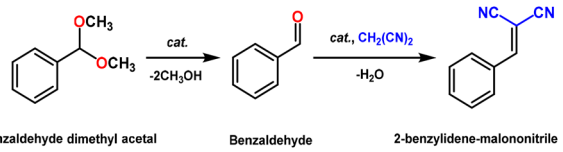

Entry	NUC-55 (mol%)	Time (h)	Temp. (°C)	Yield[b] (%)	TON[c]	TOF[d]
1	0	12	40	3	—	—
2	0.10	12	40	36	360	30
3	0.15	12	40	47	313	26
4	0.20	12	40	61	305	25
5	0.25	12	40	71	284	24
6	0.30	12	40	76	253	21
7	0.30	12	45	81	270	23
8	0.30	12	50	89	297	25
9	0.30	12	55	96	320	27
10	0.30	10	60	98	327	33
11	0.30	8	65	99	330	41
12	0.30	6	70	99	330	55

[a] Reaction conditions: benzaldehyde dimethyl acetal (10 mmol), malononitrile (20 mmol), DMSO 3 mL. [b] Product yield was determined using GC-MS with n-dodecane as an internal standard. [c] TON (turnover number) = mole of product/mole of catalyst. [d] TOF (turnover frequency) = TON/time.

factor influencing the effects of different substituted groups on reaction efficiency. Nevertheless, due to its large channel size, NUC-55 could still promote cycloaddition reactions of BDA derivatives with larger reactive substrates (entries 9 and 10 in Table S6†), with yields reaching 95% and 92%, respectively (Table 4). The results indicate that NUC-55 could effectively catalyze the deacetalization-Knoevenagel condensation reaction.[67,68] In addition, the structures of deacetalization-Knoevenagel condensation products were confirmed using ^1H NMR and ^{13}C NMR (Fig. S24–S33†).

Table 4 Effects of NUC-55 on the deacetalization-Knoevenagel condensation reaction of benzaldehyde dimethyl acetal derivatives containing different substituted groups[a]

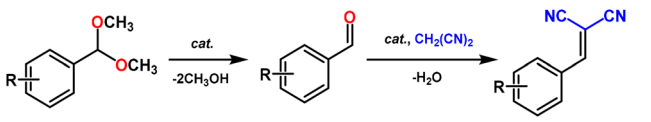

Entry	Substrates	Selectivity (%)	Yield[b] (%)	TON[c]
1	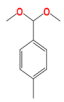	99	99	330
2		99	99	330
3	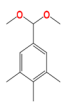	98	99	330
4	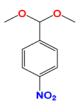	99	99	330
5	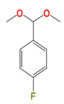	99	99	330
6	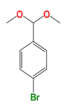	99	99	330
7		99	98	327
8	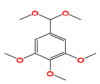	98	97	323
9	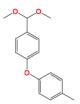	98	95	317
10	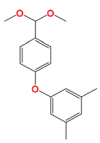	97	92	307

[a] Reaction condition: catalyst NUC-55 (0.30 mol%, based on the active {Ho_2} cluster), malononitrile (20 mmol), benzaldehyde dimethyl acetal derivatives (10 mmol), malononitrile (20 mmol), DMSO 3 mL, 70 °C, 6 h. [b] Product yield was determined using GC-MS with *n*-dodecane as an internal standard. [c] TON (turnover number) = mole of product/mole of catalyst.

2.9 Recyclability and heterogeneity of NUC-55 in the deacetalization-Knoevenagel condensation reaction

Finally, the recyclability and heterogeneity of **NUC-55** in the tandem decondensation-Knoevenagel condensation reaction were studied using BDA and malononitrile as substrates under the optimal reaction condition. After 6 h of reaction, **NUC-55** was collected through filtration, washed with methanol, and reused directly in the next catalytic cycle. As shown in Fig. S34,† the yields remained nearly unchanged during five catalytic cycles, indicating that **NUC-55** had excellent recyclability. Moreover, the PXRD patterns of recycled and original **NUC-55** showed similar characteristic diffraction peaks (Fig. S35†), indicating that the skeleton of **NUC-55** was not damaged and **NUC-55** had excellent stability and recyclability. Moreover, this can be observed from the SEM images before and after the catalytic Knoevenagel of **NUC-55** (Fig. S36†). The low-temperature N_2 adsorption experiment showed that the amount of N_2 uptake by recycled **NUC-55** was almost the same as that of original **NUC-55** (Fig. 4), indicating that **NUC-55** had high stability. In addition, the heterogeneous properties of **NUC-55** were investigated by removing it in the deacetalization-Knoevenagel condensation reaction. As shown in Fig. S37,† when **NUC-55** was removed after 2 h of reaction, the reaction was almost terminated. Meanwhile, the result of ICP-MS showed that there was a few amount of Ho^{3+} ions (0.012%) in the filtrate, which explained the slight increase in the yield at 6 h.

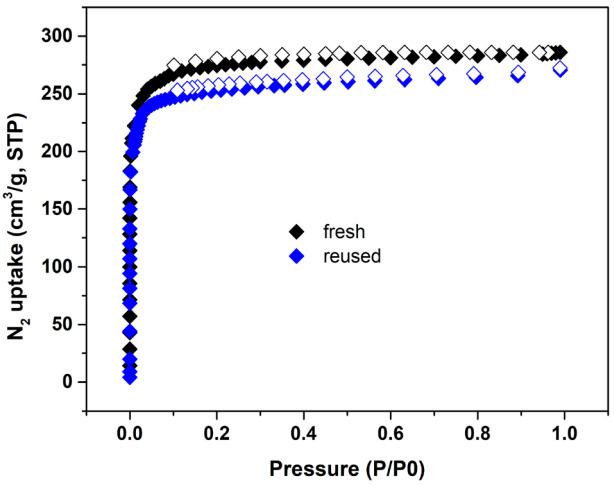

Fig. 4 N_2 adsorption isotherms of NUC-55 before and after five catalytic cycles of deacetalization-Knoevenagel condensation reactions.

2.10 Possible mechanism of the catalytic activity of NUC-55 in the deacetalization-Knoevenagel condensation reaction

Based on the structural features of **NUC-55** and relevant literature,[69–71] we proposed a possible catalytic mechanism of **NUC-55** (Fig. 5). First, BDA was hydrolyzed to benzaldehyde with the help of Lewis acidic sites of Ho^{3+} ions. Second, the oxygen atom on the aldehyde group was coordinately activated by the Lewis acidic sites of Ho^{3+} ions. Meanwhile, the methylene group of malononitrile was activated by Lewis basic sites, including the oxygen atom of the carbonyl group and the adjacent N-atom of pyridine. Third, the intermediate 1-phenyl-2,2′-dicyanoethanol was formed. Finally, benzonitrile products were formed

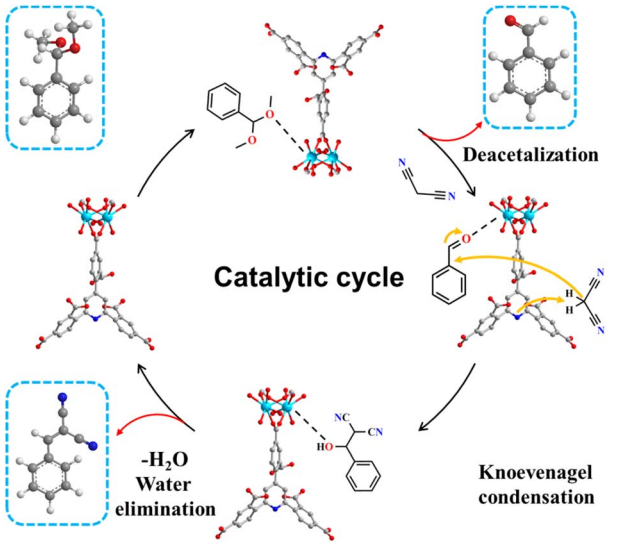

Fig. 5 Proposed catalytic mechanisms of **NUC-55** in the deacetalization-Knoevenagel condensation reaction.

after eliminating water molecules, then **NUC-55** was released and could be reused in the next cycle.[72]

3 Conclusions

In conclusion, the solvothermal self-assembly of Ho^{3+} ions and structure-oriented 2,4,6-tri(2,4-dicarboxyphenyl)pyridine (H_6TDP) ligand was used to fabricate **NUC-55**, a highly robust {Ho_2}–organic frameworks with embedded hierarchical tetragonal-microporous and octagonal-nanoporous channels. **NUC-55** possessed a plentiful of coexisted Lewis acid-base sites in its inner wall, including defective Ho^{3+} sites, carbonyl oxygen atoms, and $N_{pyridine}$ atoms. **NUC-55** showed high catalytic activity for THE cycloaddition of CO_2 to epoxides under mild conditions, with high turnover numbers and turnover frequencies. Moreover, as a heterogeneous catalyst, activated **NUC-55** could remarkably accelerate the deacetalization-Knoevenagel condensation of benzaldehyde, dimethylacetal and malononitrile. Thus, this work provides an effective synthetic route for constructing hierarchically porous Ln–organic frameworks, which not only could be used as a robust catalyst, but also could serve as a platform in various fields, such as energy storage, gas adsorption/separation, composite container, *etc.*

Data availability

All experimental datasets, including crystallographic data, are available in the Cambridge Crystallographic Data Centre (CCDC) under deposition numbers 2125269. These data can be accessed free of charge *via* [https://www.ccdc.cam.ac.uk/structures/]. Additional supporting data are provided in the ESI.†

Conflicts of interest

The authors have no relevant financial or non-financial interests to declare.

Acknowledgements

This work was financially supported by Fundamental Research Program of Shanxi Province (no. 202203021221233), Scientific and Technological Innovation Programs of Higher Education Institutions in Shanxi (no. 2022L519), and Taiyuan Institute of Technology Scientific Research Initial Funding (no. 2023KJ019).

References

1 J. Liu, Y. Zhao, L. L. Dang, G. P. Yang, L. F. Ma, D. S. Li and Y. Y. Wang, *Chem. Commun.*, 2020, **56**, 8758–8761.
2 Y. Feng, L. Zhou, H. Ma, Z. Wu, Q. Zhao, H. Li and J. Chen, *Energy Environ. Sci.*, 2022, **15**, 1711–1759.
3 H. Daglar, H. C. Gulbalkan, G. Avci, G. O. Aksu, O. F. Altundal, C. Altintas, I. Erucar and S. Keskin, *Angew. Chem., Int. Ed.*, 2021, **60**, 7828–7837.
4 L. Zeng, Y. Cao, Z. Li, Y. Dai, Y. Wang, B. An, J. Zhang, H. Li, Y. Zhou, W. Lin and C. Wang, *ACS Catal.*, 2021, **11**, 11696–11705.
5 H. R. Fu, N. Wang, X. X. Wu, F. F. Li, Y. Zhao, L. F. Ma and M. Du, *Adv. Opt. Mater.*, 2020, **8**, 202000330.
6 X. Gao, R. Cui, G. Jia and Z. Liu, *Nanoscale*, 2018, **10**, 6205–6211.
7 L. Wang, H. Qi, B. Gao, Y. Liu, H. Liu and J. Chen, *Mater. Horiz.*, 2022, **9**, 1002–1009.
8 C. I. Ezugwu, B. Mousavi, M. A. Asraf and Z. Luo, *J. Catal.*, 2016, **344**, 445–454.
9 X. K. Wang, J. Liu, L. Zhang, L. Z. Dong, S. L. Li, Y. H. Kan, D. S. Li and Y. Q. Lan, *ACS Catal.*, 2019, **9**, 1726–1732.
10 Z. S. Zhao, Y. Zhang, T. Fang, Z. B. Han and F. S. Liang, *ACS Appl. Nano Mater.*, 2020, **3**, 6316–6320.
11 B. Parmar, P. Patel, V. Murali, Y. Rachuri, R. I. Kureshy, N. H. Khan and E. Suresh, *Inorg. Chem. Front.*, 2018, **5**, 2630–2640.
12 M. Ding, X. Cai and H. L. Jiang, *Chem. Sci.*, 2019, **10**, 10209–10230.
13 X. G. Yang, Z. M. Zhai, L. F. Ma and D. P. Yan, *ACS Cent. Sci.*, 2020, **6**, 1169–1178.
14 Y. Shi, J. Zhao, H. Xu, S. L. Hou and B. Zhao, *Sci. China Chem.*, 2021, **64**, 1316–1322.
15 C. S. Cao, Y. Shi, H. Xu and B. Zhao, *Chem. Commun.*, 2021, **57**, 7537–7540.
16 W. Zhou, D. D. Huang, Y. P. Wu, J. Zhao, T. Wu, J. Zhang, D. S. Li, C. Sun, P. Feng and X. Bu, *Angew. Chem., Int. Ed.*, 2019, **58**, 4227–4231.
17 G. Avci, I. Erucar and S. Keskin, *ACS Appl. Mater. Interfaces*, 2020, **12**, 41567–41579.
18 P. Z. Li, X. J. Wang, J. Liu, H. S. Phang, Y. Li and Y. Zhao, *Chem. Mater.*, 2017, **29**, 9256–9261.
19 C. Wang, B. An and W. Lin, *ACS Catal.*, 2019, **9**, 130–146.
20 H. Zhang, Z. Li, J. Wang, C. Wang, J. Dong, G. Liu, S. Gong, L. Shi, R. Dong and X. Huang, *J. CO_2 Util.*, 2024, **82**, 102760.
21 J. F. Kurisingal, Y. Rachuri, A. S. Palakkal, R. S. Pillai, Y. Gu, Y. Choe and D. W. Park, *ACS Appl. Mater. Interfaces*, 2019, **11**, 41458–41471.

22 X. Huang, X. Gu, H. Zhang, G. Shen, S. Gong, B. Yang, Y. Wang and Y. Chen, *J. CO_2 Util.*, 2021, **45**, 101419.
23 J. Liu, G. P. Yang, J. Jin, D. Wu, L. F. Ma and Y. Y. Wang, *Chem. Commun.*, 2020, **56**, 2395–2398.
24 J. Liu, Y. Z. Fan, X. Li, Y. W. Xu, L. Zhang and C. Y. Su, *ChemSusChem*, 2018, **11**, 2340–2347.
25 X. Huang, Y. Chen, Z. Lin, X. Ren, Y. Song, Z. Xu, X. Dong, X. Li, C. Hu and B. Wang, *Chem. Commun.*, 2014, **50**, 2624–2627.
26 P. Das and S. K. Mandal, *ACS Appl. Mater. Interfaces*, 2020, **12**, 37137–37146.
27 J. Liu, Y. Wei and Y. Zhao, *ACS Sustainable Chem. Eng.*, 2019, **7**, 82–93.
28 S. L. Hou, J. Dong, X. L. Jiang, Z. H. Jiao and B. Zhao, *Angew. Chem., Int. Ed.*, 2019, **58**, 577–581.
29 E. Liu, J. Zhu, W. Yang, F. Liu, C. Huang and S. Yin, *ACS Appl. Nano Mater.*, 2020, **3**, 3578–3584.
30 Z. Zhang, J. Ye, T. Ju, L. L. Liao, H. Huang, Y. Y. Gui, W. J. Zhou and D. G. Yu, *ACS Catal.*, 2020, **10**, 10871–10885.
31 X. Yang, Q. Zou, T. Zhao, P. Chen, Z. Liu, F. Liu and Q. Lin, *ACS Sustainable Chem. Eng.*, 2021, **9**, 10437–10443.
32 H. R. Zhang, J. Z. Gu and A. M. Kirillov, *Inorg. Chem. Front.*, 2021, **8**, 4209–4221.
33 Y. Yang, C. Y. Gao, H. R. Tian, J. Ai, X. Min and Z. M. Sun, *Chem. Commun.*, 2018, **54**, 1758–1761.
34 D. Yang and B. C. Gates, *ACS Catal.*, 2019, **9**, 1779–1798.
35 H. Chen, L. Fan and X. Zhang, *ACS Appl. Nano Mater.*, 2020, **3**, 7201–7210.
36 H. Chen, L. Fan and X. Zhang, *ACS Appl. Mater. Interfaces*, 2020, **12**, 54884–54892.
37 H. Chen, L. Fan, T. Hu and X. Zhang, *Inorg. Chem.*, 2021, **60**, 3384–3392.
38 H. T. Chen, T. P. Hu, L. M. Fan and X. T. Zhang, *Inorg. Chem.*, 2021, **60**, 1028–1036.
39 J. M. Gu, X. D. Sun, X. Y. Liu, Y. Yuan, H. Y. Shan and Y. L. Liu, *Inorg. Chem. Front.*, 2022, **22**, 4517–4526.
40 X. Y. Chen, B. Zhao, W. Shi, J. Xia, P. Cheng, D. Z. Liao, S. P. Yan and Z. H. Jiang, *Chem. Mater.*, 2005, **17**, 2866–2874.
41 J. X. Liao, W. J. Zeng, B. S. Zheng, X. Y. Cao, Z. X. Wang, G. Y. Wang and Q. Y. Yang, *Inorg. Chem. Front.*, 2022, **9**, 1939–1948.
42 J. Lyu, X. Zhang, P. Li, X. Wang, C. T. Buru, P. Bai, X. Guo and O. K. Farha, *Chem. Mater.*, 2019, **31**, 4166–4172.
43 R. Vismara, G. Tuci, N. Mosca, K. V. Domasevitch, C. D. Nicola, C. Pettinari, G. Giambastiani, S. Galli and A. Rossin, *Inorg. Chem. Front.*, 2019, **2**, 533–545.
44 T. Zhang, H. Chen, S. Liu, H. Lv, X. Zhang and Q. Li, *ACS Catal.*, 2021, **11**, 14916–14925.
45 H. Chen, S. Liu, H. Lv, Q.-P. Qin and X. Zhang, *ACS Appl. Mater. Interfaces*, 2022, **14**, 18589–18599.
46 P. Pachfule and R. Banerjee, *Cryst. Growth Des.*, 2012, **12**, cg300827e.
47 Y. Zhao, J. Qiu, Z. Li, H. Wang and J. Wang, *ACS Sustainable Chem. Eng.*, 2020, **8**, 18413–18419.
48 Y. H. Zou, Y. B. Huang, D. H. Si, Q. Yin, Q. J. Wu, Z. Weng and R. Cao, *Angew. Chem.*, 2021, **133**, 2–8.
49 Y. J. Li, Y. L. Wang and Q. Y. Liu, *Inorg. Chem.*, 2017, **56**, 2159–2164.
50 T. Q. Song, K. Yuan, W. Z. Qiao, Y. Shi, J. Dong, H. L. Gao, X. P. Yang, J. Z. Cui and B. Zhao, *Anal. Chem.*, 2019, **91**, 2595–2599.
51 Y. Zhang, Y. Wang, L. Liu, N. Wei, M. L. Gao, D. Zhao and Z. B. Han, *Inorg. Chem.*, 2018, **57**, 2193–2198.
52 X. Shi, B. Cao, J. Liu, J. Zhang and Y. Du, *Small*, 2021, **17**, 2005371.
53 S. W. Zhang, F. X. Ou, S. G. Ning and P. Cheng, *Inorg. Chem. Front.*, 2021, **7**, 1865–1899.
54 S. Zhang, F. Ou, S. Ning and P. Cheng, *Inorg. Chem. Front.*, 2021, **8**, 1865–1899.
55 Y. Zhang, S. Liu, Z. S. Zhao, Z. F. Wang, R. Y. Zhang, L. Liu and Z. B. Han, *Inorg. Chem. Front.*, 2021, **3**, 590–619.
56 G. Shi, W. Xu, J. Wang, Y. Yuan, S. Chaemchuen and F. Verpoort, *J. CO_2 Util.*, 2020, **39**, 101177.
57 Z. Zhou, J. G. Ma, J. Gao and P. Cheng, *Green Chem.*, 2021, **23**, 5456–5460.
58 X. K. Wang, J. Liu, L. Zhang, L. Z. Dong, S. L. Li, Y. H. Kan, D. S. Li and Y. Q. Lan, *ACS Catal.*, 2019, **9**, 1726–1732.
59 K. Liu, S. Jiao, H. Zhao, F. Cao and D. Ma, *Green Chem.*, 2021, **23**, 1766–1771.
60 A. Shaabani, R. Mohammadian, H. Farhid, M. K. Alavijeh and M. M. Amini, *Ind. Eng. Chem. Res.*, 2019, **58**, 2784–2791.
61 F. Norouzi and H. R. Khavasi, *ACS Omega*, 2019, **4**, 19037–19045.
62 P. Das and S. K. Mandal, *ACS Appl. Mater. Interfaces*, 2020, **12**, 37137–37146.
63 Y. B. N. Tran, P. T. K. Nguyen, Q. T. Luong and K. D. Nguyen, *Inorg. Chem.*, 2020, **59**, 16747–16759.
64 Y. Li, X. Zhang, J. Lan, D. Li, Z. Wang, P. Xu and J. Sun, *ACS Sustainable Chem. Eng.*, 2021, **9**, 2795–2803.
65 G. Jin, D. Sensharma, N. Zhu, S. Vaesen and W. Schmitt, *Dalton Trans.*, 2019, **48**, 15487–15492.
66 B. Parmar, P. Patel, R. S. Pillai, R. I. Kureshy, N. H. Khan and E. Suresh, *J. Mater. Chem. A*, 2019, **7**, 2884–2894.
67 F. Norouzi and H. R. Khavasi, *ACS Omega*, 2019, **4**, 19037–19045.
68 A. Shaabani, R. Mohammadian, H. Farhid and M. K. Alavijeh, *Ind. Eng. Chem. Res.*, 2019, **58**, 2784–2791.
69 C. I. Ezugwu, B. Mousavi, M. A. Asraf, Z. Luo and F. Verpoort, *J. Catal.*, 2016, **344**, 445–454.
70 X. Y. Dao and W. Y. Sun, *Inorg. Chem. Front.*, 2021, **13**, 3178–3204.
71 P. P. Mondal, S. Sarkar, M. Singh and S. Neogi, *ACS Sustainable Chem. Eng.*, 2024, **12**(42), 15432–15446.
72 Y. Yao, K. X. Huang, Y. Liu, T. T. Luo, G. Tian, J. X. Li, S. Zhang, G. G. Chang and X. Y. Yang, *Inorg. Chem. Front.*, 2021, **14**, 3463–3472.